The Journal of Chemical Physics

RESEARCH ARTICLE | MAY 16 2025

UV-photoelectron spectroscopy and MS-CASPT2/CASSCF study of the thermolysis of azidoethyl-methyl sulfide: Characterization and mechanism of the formation of *S*-methyl-*N*-sulfenylethanimine

Manuel Algarra ; Stephane Labat ; José Enrique Rodríguez-Borges ; María Soledad Pino-González ; Jean Marc Sotiropoulos ; Juan Soto

J. Chem. Phys. 162, 194303 (2025)
https://doi.org/10.1063/5.0261967

The Journal of Chemical Physics ARTICLE pubs.aip.org/aip/jcp

UV-photoelectron spectroscopy and MS-CASPT2/CASSCF study of the thermolysis of azidoethyl-methyl sulfide: Characterization and mechanism of the formation of *S*-methyl-*N*-sulfenylethanimine

Cite as: J. Chem. Phys. 162, 194303 (2025); doi: 10.1063/5.0261967
Submitted: 31 January 2025 • Accepted: 28 April 2025 •
Published Online: 16 May 2025

Manuel Algarra,[1,a] Stephane Labat,[2,a] José Enrique Rodríguez-Borges,[3] María Soledad Pino-González,[4,5] Jean Marc Sotiropoulos,[2] and Juan Soto[5,6,a]

AFFILIATIONS

[1] Department of Science,INAMAT[2]-Institute for Advanced Materials and Mathematics, Campus de Arrosadia, 31006 Pamplona, Spain
[2] Université de Pau et des Pays de l'Adour, CNRS, IPREM, Technopole Helioparc-2, Av. Pdt P. Angot, 64053 Pau Cedex 09, France
[3] LAQV/REQUIMTE, Department of Chemistry and Biochemistry, Faculty of Sciences of University of Porto, 4169-007 Porto, Portugal
[4] Department of Organic Chemistry, Faculty of Science, University Málaga, Málaga, Spain
[5] University Institute of Materials and Nanotechnology (IMANA), University of Málaga, Campus de Teatinos, 29071 Málaga, Spain
[6] Department of Physical Chemistry, Faculty of Science, University of Málaga, Andalucía Tech., E-29071 Málaga, Spain

[a] **Authors to whom correspondence should be addressed:** manuel.algarra@unavarra.es; stephane.labat@univ-pau.fr; and soto@uma.es

ABSTRACT

The thermal decomposition of azidoethyl methyl sulfide was studied by real-time UV-photoelectron spectroscopy (UV-PES) at temperatures ranging from 773 to 1023 K. Different ionization energies were obtained using density functional theory calculations to assign UV-PES spectra. The complete active space self-consistent field and multistate second-order perturbation methods were used to predict the formation of different species present in the thermal decomposition process. N_2 and *S*-methyl-*N*-sulfenylethanimine are generated at 773 K. The first step of the reaction is the dissociation of the molecule into nitrene and nitrogen. The spin state (singlet or triplet) of nitrene formed in the first step of the reaction is temperature-dependent. At low temperatures ($T \leq 650$ K), both states are formed with almost the same probability; in contrast, at high temperatures ($T \geq 1000$ K), singlet nitrene is the majority intermediate. From this singlet nitrene, three stable reaction products were detected in the experiments: an imine derivative, a four-member cyclic derivative, and a sulfenyl derivative.

I. INTRODUCTION

Organic azide derivatives (X-N_3) are significant in many different areas of chemistry, including materials science,[1] biological[2,3] organic synthesis, and click chemistry.[4,5] The azide molecule mostly functions as a co-reactant or a generator of intermediates, such as nitrenes, in diverse processes,[6] or imines, which are formed by thermolysis or photolysis of the parent azide.[7–9]

Sulfenylimine derivatives (R = **N**-**S**-R) are not very common compounds but are considered effective intermediates for organic synthesis.[10,11] Thus, a variety of synthetic processes have been referenced considering their unique chemical reactivity due to the

presence of an imino group and a sulfur–nitrogen bond.[11] We can highlight procedures starting from sulfenamides and aldehydes or ketones,[12] oximes with Bu_3P and PhSSPh,[13] or oximes in Cu-catalyzed reactions.[14] Other starting materials, such as amines and thiols, have been transformed into *N*-sulfenylimines using an electrochemical approach mediated by thiophenols and bromide ions, respectively.[15,16] Another useful synthesis route was discovered to generate them as intermediates in the formation of relevant sulfonamides. The corresponding *N*-sulfenylimines were formed from α-iminomalonates due to their *N*-centered umpolung reactivity.[17]

Our group used the photochemical breakdown of organic sulfide azides [R-S-$(CH_2)_n$-N_3] to obtain *N*-sulfenylimines in a process where the nitrene intermediate was found to be the key point.[18] Recently, we have obtained *N*-sulfenylimines from azidomethyl methyl sulfide (AMMS).[18] In the present work, we aimed to study the thermal decomposition of an organic sulfide azide, azidoethyl methyl sulfide (AEMS). To achieve this objective, we applied UV-photoelectron spectroscopy (UV-PES) and multiconfigurational *ab initio* theoretical methods [complete active space self-consistent field (CASSCF) and multistate second-order perturbation (MS-CASPT2)]. UV-PES allowed us to identify the main reaction products of AEMS decomposition: nitrene, imine, and sulfenylimine. However, computations performed at high levels of theory allowed us to establish the reaction mechanisms for the formation of each intermediate.[18]

II. EXPERIMENT

A. Synthesis and characterization of AEMS

An Ar atmosphere was used to stir a mixture of 1-chloroethylmethylsulfide (1.00 g; 9.02 mmol), NaN_3 (2.93 g; 45.1 mmol), and acetone (50 ml) for three days at 56 °C. After bringing the reaction mixture to room temperature, 100 ml of diethyl ether and water were added. After separation, the organic layer was cleaned three times using 100 ml of brine. After drying over Na_2SO_4, the organic extract was filtered. After the solvent was removed using a moderate vacuum (water tube) at room temperature, a colorless liquid (1.04 g, 98%) known as azide (AEMS) was obtained. ^{13}C NMR ($CDCl_3$): δ = 16.12 (CH_3); 33.73 (S-CH_2); 51.06 (N_3-CH_2). ^1H NMR ($CDCl_3$): δ = 2.15 (*s*, 3H, S-CH_3); 2.69 (*t*, 2H, J = 6.96 Hz, S-CH_2); 3.46 (*t*, 2H, *J* = 6.96 Hz, N_3-CH_2). Analyzed: C, 30.75; H, 6.02; N, 35.86; S, 27.37 for $C_3H_7N_3S$.

B. Experimental details of UV-photoelectron spectroscopy

1. Instrumentation and methodology for UV-photoelectron spectroscopy

A three-part in-house spectrometer designed by IPREM and fitted with a 127° cylindrical analyzer and a He-I radiation source (21.21 eV and/or 48 eV) was used to record the UV-PES spectra. The instrument operated at a pressure of 5 × 10 hPa, while the pressure for the channeltron (X914L) was maintained at ≤10 hPa. Monitoring was performed using a microcomputer coupled with a digital-to-analog converter (AEI spectrum). The spectra resulting from a single scan consisted of 2048 points, with an accuracy of 0.05 eV. Calibration was achieved using Xe lines (12.13 and 13.44 eV) and Ar lines (15.76 and 15.94 eV). The precision of the ionization energies was ±0.05 eV for broad or overlapping signals and ±0.03 eV for acute peaks. AEMS samples were introduced into the spectrometer via a vaporization oven, where they were slowly vaporized at a low pressure (1.3×10^{-6} hPa) within a handmade three-valve injector (3/4-in. diameter, 10 cm length, operating temperature: 145 K ≤ T ≤ 573 K) by flash vacuum thermolysis (FVT). During thermolysis, the vaporized samples were gradually heated to the desired temperature using a second oven, and the UV-PES spectra were recorded at each temperature increment. Special attention was paid to ensuring the stability of the temperature and pressure during each measurement to obtain reproducible and accurate results. It has also been obtained by the flash vacuum thermolysis (FVT).

2. Thermolysis procedure

Thermolysis experiments were performed using a dual oven system. The spectrometer was connected to a vacuum line, maintaining a pressure of 1.3×10^{-6} mbar. The first oven, operated at 298 K, was used to vaporize the sample slowly, generating a diluted and stable gas flow. This oven was particularly effective for handling volatile precursors, such as AEMS. The second oven was responsible for conducting the thermolysis, with temperatures ranging from 773 to 1023 K. To ensure that reactive intermediates could rearrange and reach more thermodynamically stable configurations, the vacuum line was extended by 50 cm and maintained at 573 K. This setup allowed for the isolation and characterization of stable species formed during the thermal decomposition of AEMS.

C. Calculation methods

1. Interpretation of UV-PES data

To interpret the UV-PES data, computational studies were performed using density functional theory (DFT) for closed-shell species. In contrast, for open-shell species, such as nitrenes, multiconfigurational wavefunction methods were applied (see further below) because the singlet nitrene species cannot be treated with conventional DFT methods. All DFT calculations were performed using the Gaussian 16 computational package.[19] These calculations were essential for assigning ionization energies and providing a detailed understanding of the electronic structure of the thermolysis products. For the closed-shell species, the CAM-B3LYP[20–23] functional combined with the 6-311++G(d,p) basis set was used.[24] In previous studies, this method has been shown to produce reliable results for similar systems. To assign the first bands in the UV-PES spectra, we applied the method developed by Muchall *et al.*[25] and Muchall and Rademacher,[26] which involves a correction to the Kohn–Sham orbital energies (ε_{KS}). For that, we uniformly shifted all eigenvalues such that the highest occupied molecular orbital (HOMO) energy matched the first vertical ionization potential. The ionization potential of the HOMO (IP_{HOMO}) is defined as IP_{HOMO} (eV) = $E_{cation} - E_{neutral}$, where $E_{neutral}$ is the total energy of the neutral species and E_{cation} is the total energy of the ionized molecule computed at the neutral geometry. To align the HOMO energy with the ionization potential, a uniform energy shift was introduced, $\Delta_{shift} = IP_{HOMO} + \varepsilon_{HOMO}$. This shift was then applied to all KS orbital energies to refine the higher ionization potentials (ε_i^{Corr}).

2. Theoretical elucidation of the decomposition of AEMS by MS-CASPT2

The CASSCF[27–33] and MS-CASPT2[34,35] methods were applied as implemented in the MOLCAS 8.6 program.[36,37] MS-CASPT2

energies were calculated on top of the optimized CASSCF geometries. To prevent the inclusion of invader states in such calculations, an imaginary shift set to 0.1 was used. A standard value (0.25) for the IPEA empirical correction was applied to each calculation. The CASSCF computations utilizing the state-average approach are abbreviated as SAn-CASSCF, where n is the number of states of a certain symmetry species. The minimum energy crossing points of different spin multiplicities (i.e., intersystem crossings) and conical intersections were optimized with the algorithms[38] implemented in MOLCAS. The so-called ANO-RCC basis sets,[39,40] that is, extended relativistic basis sets of the atomic natural orbital (ANO)-type, were used in this study's multiconfigurational calculations by applying the contraction scheme (S)[5*s*4*p*3*d*2*f*1*g*]/(C,N,O)[4*s*3*p*2*d*1*f*]/(H)[3*s*2*p*1*d*]. The molecular orbitals and geometries of the chemical species were analyzed using the programs Gabedit[41] and Molden,[42] and the analysis of vibrational normal modes, including saddle point (transition vector) conical intersections (derivative coupling and energy difference gradient vectors) and intersystem crossings (energy difference gradient vector), was carried out using the program MacMolplt.[43] The values of the spin–orbit coupling constants between S_0 and T_0 were computed using a one-electron spin–orbit Fock-type Hamiltonian.[44–46] The convention followed to label the electronic states is the energetic order within each multiplicity at the geometry of the ground state; that is, the states are labeled as S_0, S_1, …, S_n for singlet states and T_0, T_1, …, T_n for triplet states. An accurate 1D representation of the potential energy surface in the space spanned by the set of internal coordinates that define the molecular geometry is provided by the interpolation method,[47–50] which is used to build the 1D potential energy surfaces for dissociation and isomerization reactions using the full space of non-redundant internal coordinates. To accomplish this, a common set of 3N-6 internal coordinates was established for the reactant ($\mathbf{R_1}$), product(s) ($\mathbf{R_2}$), and target geometries. Our experience with dissociation reactions indicates that the asymptotic limit of the potential energy surface of interest can be reached at a separation distance of 4.7 Å of the dissociative bond. Second, an interpolation vector ($\mathbf{R}$) that links the reactants and products was produced by the difference between $\mathbf{R_2}$ and $\mathbf{R_1}$. Third, $\mathbf{R}$ was divided by n, which can be whatever integer the user chooses. Each division is referred to as a step. Consequently, $\mathbf{R_m} = \mathbf{R_1} + \mathbf{(m/n)/R}$ represents the nuclear configuration corresponding to each step m. We were unable to provide a distinct unit for the reaction coordinates because we employed internal coordinates (dihedral angles, valence bonds, and internuclear distances). Thus, the units used in the interpolations were arbitrary. There are two advantageous features of linear interpolation in internal coordinates: (i) it requires less computing power than a scan with geometry relaxation and (ii) every point along the reaction coordinate or interpolation vector must be on a straight line. However, if the potential energy surfaces are scanned with geometry relaxation, this is not the case. The constant rates associated with intersystem crossings (non-adiabatic reactions) and transition states (adiabatic reactions) were determined using the program MESMER v.5.2.[51–55] The microcanonical rate coefficients of ISCs were calculated using the Landau–Zener[56,57] model, and the transition state microcanonical rate constants were calculated using the Rice–Ramsperger–Kassel–Marcus theory.[58–62]

3. Data analysis

The collected UV-PES data were analyzed using both experimental and theoretical approaches. For each spectrum, the energies of the ionization bands were compared with the theoretical predictions obtained from DFT and CASSCF calculations. This comparison allowed the assignment of molecular orbitals to specific ionization events, providing a detailed picture of the electronic structure of the species formed during thermolysis. The correlation between the experimental and theoretical ionization energies is essential for identifying key intermediates, such as nitrene and imine species, and for understanding the reaction mechanism of AEMS thermolysis.

III. RESULTS AND DISCUSSION

The thermolysis of AEMS was studied using UV-PES, which provided valuable insights into the electronic structures of the reaction products at different temperatures.

A. UV-PES spectroscopy

1. UV-PES spectra of M1

The initial spectrum was recorded for the azide precursor (**M1**, Fig. 1), which was vaporized at 298 K. The UV-PES spectrum of M1 shows three prominent ionization bands at 8.8, 9.7, and 11.2 eV, corresponding to different molecular orbitals (Table I).

The first band (8.8 eV) is attributed to the ionization of the HOMO, which is primarily localized on the sulfur lone pair (Lp S). The second band (9.7 eV) corresponds to the ionization of a nonbonding orbital (HOMO-1) formed by the combination of 2p atomic orbitals on nitrogen atoms N1 and N2. The third band at 11.2 eV, which is broader and more intense,

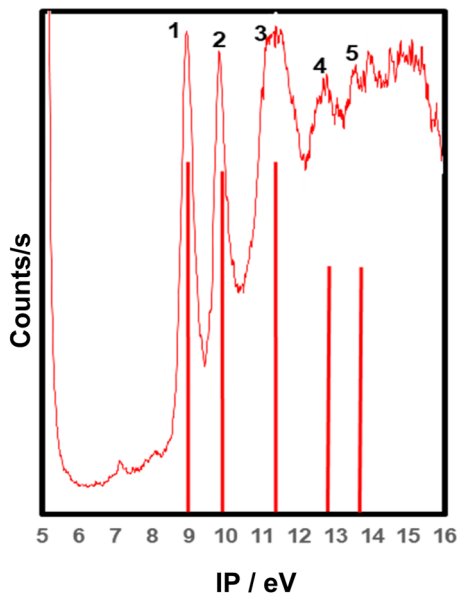

FIG. 1. UV-photoelectron spectra of M1. Theoretical ionization energies (vertical lines: position).

TABLE I. Corrected IP of MOs ε_i^{Corr} with GaussView MO visualizations for M1 in comparison with experimental values (in eV).

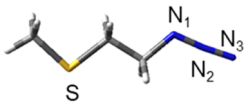

Nature of MOs		ε_i^{Corr}	Exp. IP
1	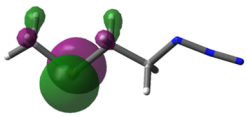	8.9	8.8
2	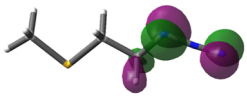	9.8	9.7
	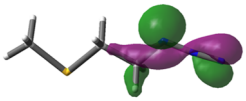	11.2	11.2
3	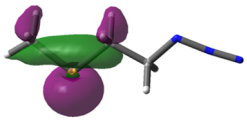	11.4	⋯
4	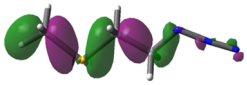	12.8	12.6
5	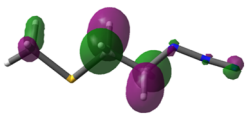	13.3	13.4

is associated with an antibonding interaction between N1 and the weak orbitals of N2 and N3. These assignments are supported by theoretical calculations performed using the CAM-B3LYP/6-311++G(d,p) method. The calculated ionization energies aligned well with the experimental values, confirming the electronic structure of M1.

2. Thermolysis at 773 K: Formation of (Z)-S-methyl-N-sulfenylethanimine

At 773 K, a new UV-PES spectrum was recorded after thermolysis of M1 (Fig. 1). The spectrum exhibits a fine band at 15.7 eV (*), corresponding to the first ionization potential of molecular nitrogen, confirming the selective cleavage of the azide group. This result indicates that thermolysis at this temperature successfully generates a new product, identified as (*Z*)-*S*-methyl-*N*-sulfenylethanimine (**M5**, Fig. 2).

This sulfenyl imine can also be named (*Z*)-*N*-ethylidene methanesulfenamide. Theoretical calculations of **M5**'s molecular orbitals further corroborate the experimental findings (Table II). The first ionization energy (8.7 eV) corresponds to the ionization of a π-type antibonding orbital between Lp S and the N_1C(Me)

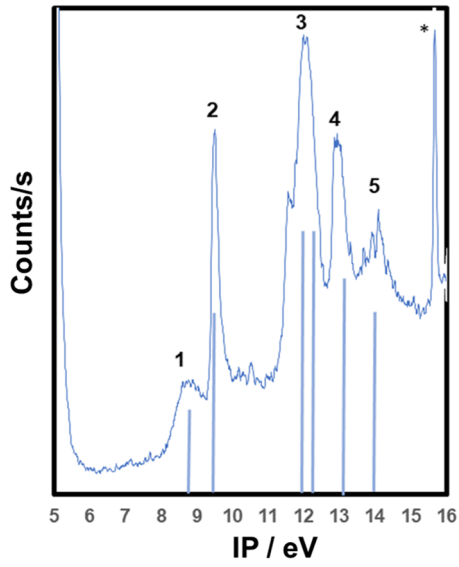

FIG. 2. FVT of AEMS at 773 K. The asterisk corresponds to the first ionization energy of N_2. Theoretical ionization energies (vertical lines: position).

π-bond. The second ionization energy (9.5 eV) was related to the interaction between the sulfur atom σ lone pair and Lp N_1. The third band observed at 12.0 eV is attributed to HOMO-2, which involves a bonding combination between Lp S and the π-bond of N_1C, and HOMO-3 with a significant contribution from the sulfur σ lone pair.

3. Thermolysis at 973 K: Detection of reactive nitrene species

Increasing the temperature to 973 K led to the further decomposition of the AEMS precursor. The resulting UV-PES spectrum displays two distinct bands: a shoulder at 7.5 eV and a sharp band at 8.7 eV (Fig. 3). These features correspond to singlet nitrene (S_0) species formed during thermolysis (Table III). Theoretical analysis using the MS-CASPT2 method identified the shoulder at 7.5 eV as originating from the free sulfur lone pair, while the band at 8.7 eV corresponds to the ionization of the nitrogen lone pair.

This confirmed the formation of a highly reactive singlet nitrene intermediate. For the triplet nitrene (T_0) species, two additional ionization bands were observed: single occupied molecular orbital (SOMO) at 9.3 eV, corresponding to the ionization of the nitrogen lone pair, and SOMO-1 (10.6 eV), associated with the ionization of the nitrogen σCN1 bond.

The presence of these ionization bands indicates the coexistence of both singlet and triplet nitrene species under experimental conditions, with the singlet species being more abundant. Theoretical analysis using the MS-CASPT2 method identified the shoulder at 7.5 eV as originating from the free sulfur lone pair, while the band at 8.7 eV corresponds to the ionization of the nitrogen lone pair. This confirmed the formation of a highly reactive singlet nitrene intermediate.

TABLE II. Corrected IP of MOs ε_i^{Corr} with GaussView MO visualizations for M5 in comparison with experimental values (in eV).

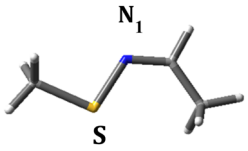

Nature of MOs	ε_i^{Corr}	Exp. IP
1	8.5	8.7
2	9.6	9.5
3	12.0	12.0
4	12.5	⋯
	13.0	13.0
5	13.9	13.9

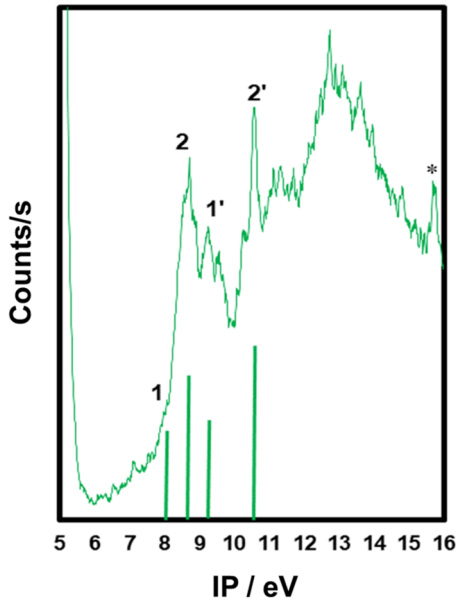

FIG. 3. FVT of AEMS at 973 K. The values (1 and 2) correspond to the singlet nitrene, whereas those with prime (1′ and 2′) correspond to the triplet nitrene. The asterisk corresponds to the first ionization energy of N_2. Theoretical ionization energies (vertical lines: position).

TABLE III. Corrected IP of MOs (ε^{Corr}) for nitrene S_0 and T_0 calculated with MS-CASPT2 in comparison with experimental values (in eV).

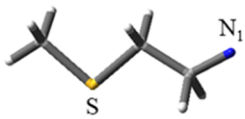

Nature of MOs	ε_i^{Corr}	Exp. IP
Singlet		
1	7.6	7.5
2	8.8	8.7
Triplet		
1	9.3	9.3
2	10.6	10.6

4. Increasing stability: Extension of the thermolysis line

To further investigate the fate of the nitrene species, the thermolysis line was extended by 50 cm and maintained at 573 K, while **M1** was thermolyzed at 1023 K. This setup allows for additional reaction times, leading to the stabilization of more thermodynamically favorable products. The UV-PES spectra recorded under these conditions revealed the formation of imine **M2** (Fig. 4).

The first ionization energy of **M2** was observed at 8.8 eV and was assigned to sulfur lone pair ionization (π plane). The second and third bands, at 10.4 and 11.2 eV, correspond to the nitrogen

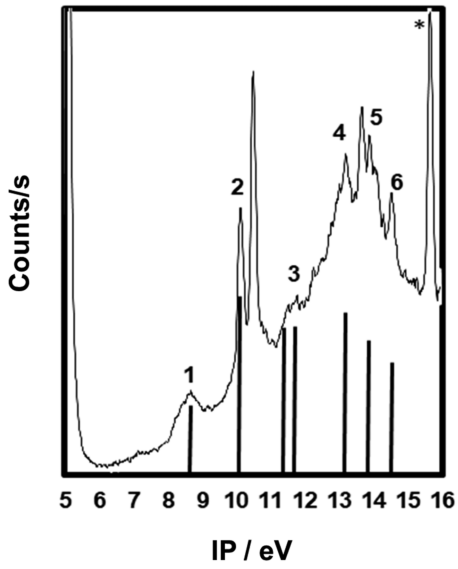

FIG. 4. FVT of AEMS at 1023 K with the thermolysis line extended by 50 cm and maintained at 573 K. The asterisk corresponds to the first ionization energy of N_2. Theoretical ionization energies (vertical lines: position).

lone pairs and the sulfur lone pair in the σ plane. The fourth band (13.1 eV) was attributed to the ejection of electrons from σ the bonds (Table IV).

B. CASSCF studies of the thermal decomposition channels of AEMS and its intermediates

Azides are strongly correlated systems based on their electronic structure.[63–65] In this context, MCSCF theories[27–34] are appropriate quantum chemical approximations to deal with this type of system, among which the CASSCF method is a particular case. To obtain a correct answer to the problem under study using the CASSCF method, the key step is the selection of the orbital subspace to be included in the multi-configurational reference wavefunction,[66,67] which is called the active space. Although various automated methods to obtain such an active space have been reported in the literature, they are not free from a trial-and-error process combined with chemical intuition to select the correct orbitals.[68,69] Thus, based on our experience with other azide derivatives,[6] the active space for studying the thermal reactions of AEMS was selected by hand and consisted of 16 electrons distributed in 13 orbitals (Fig. 5).

1. Electronic structure of AEMS

The active space comprises the following orbitals: two N (2*s*) lone pairs, two N–N–N σ bonds (σNNN), two N–N–N σ* bonds (σ*NNN), one C–N σ bond (σCN), one C–N σ* bond (σ*CN), one N–N π bond (πNN), one N–N π* bond (π*NN), one Newton-N π bond (πNNN), one N–N–N π* bond (π*NNN), and one N–N n_π bond (n_π) (Fig. 5).

TABLE IV. Corrected IP of MOs (ε^{Corr}) with GaussView MO visualizations for imine M2 in comparison with experimental values (in eV).

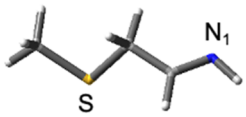

Nature of MOs		ε_i^{Corr}	Exp. IP
1	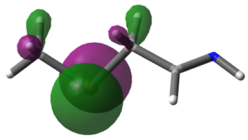	8.9	8.8
2	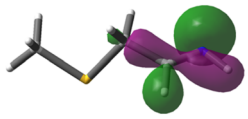	10.3	10.2
3	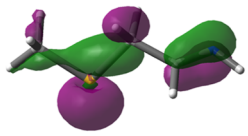	11.1	11.2
	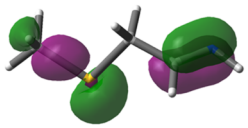	11.9	...
4	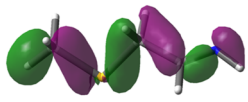	13.1	13.1
5	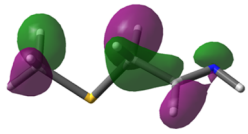	14.0	14.2
6	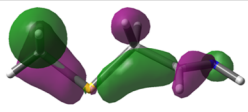	14.7	14.7

2. Dissociation of AEMS into nitrene and N_2: Reactions of the nitrene intermediate

In this section, we discuss the results of the dissociation of AEMS [Fig. 6(a)] into nitrene [Figs. 6(d)–6(f), $CH_3SCH_2CH_2N$] and molecular nitrogen.

As a starting point to understand this reaction, we computed the 2D potential energy surfaces of the lowest singlet and triplet states, which led to the dissociation of the parent molecules in their respective spin states, as depicted in Fig. 7. These curves were obtained using the interpolation method[47–50] and were computed at the MS-CASPT2 level of theory with an SA2-CASSCF

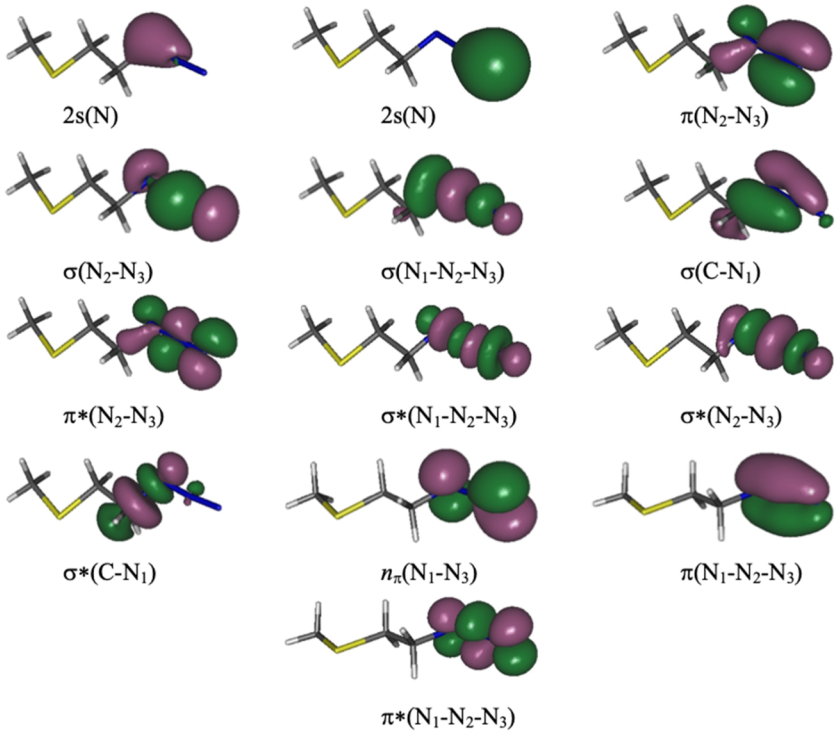

FIG. 5. CASSCF (16e,13o)/ANO-RCC molecular orbitals included in the active space of AEMS.

(16e,13o) reference wavefunction for each symmetry species under the C_s-geometry constraint.

In this context, Fig. 7 indicates that there are two dissociation channels with close energy barriers for the thermal decomposition of azide [Fig. 6(a)] into nitrene and molecular nitrogen: (i) *spin-forbidden* and (ii) *spin-allowed*. The symmetry of the lowest triplet state (T_0) of the nitrene intermediate was $1^3A''$, and the lowest singlet nitrene (S_0) was electronically configured as a closed-shell species with $1^1A'$ symmetry.

Thus, by taking as starting points those points marked in Fig. 3 as pISC1 and pTS1, we were able to optimize the minimum energy geometries of the intersystem crossing for the spin-forbidden channel [Fig. 6(b), spin–orbit coupling constant = 46.6 cm^{-1}] and the transition state for the spin-allowed one [Fig. 6(c)], respectively (the separation between these two geometries is only 0.32 Å, evaluated in Cartesian coordinates).

At this point, the probability of each channel could be estimated using the MESMER program.

The exit energy barriers of the singlet and triplet channels were 50.28 and 47.37 kcal/mol, respectively, and the dissociation energies amounted to 43.93 kcal/mol for the singlet channel and 11.07 kcal/mol for the triplet one. From an energetic perspective, both routes were almost equally probable. The ordering and proximity between the geometries of ISC1 and TS1 would favor the triplet route; that is, the nuclear velocities of the system approached zero as they entered the domain of the transition state (TS1), which in turn favored the singlet-triplet crossing via ISC1 because ISC1 and TS1 were geometrically close.[70–74]

In the temperature range of the UV-PES experiments (650–1000 K), the kinetic estimations (at the high-pressure limit) of the rate constants of the singlet and triplet channels show that, at low temperatures ($T \leq 650$ K), both routes have almost the same rate constant magnitude as the rate constant of the triplet state; in contrast, at high temperatures ($T \geq 1000$ K), the singlet channel is ~40 times more rapid than the triplet dissociation channel (Fig. 8).

It is worth noting that Fig. 6(b) shows that there were no displacements of the α-H atoms in the normal mode associated with the imaginary frequency of the transition state TS0 (first step of the reaction). Furthermore, the quantitative estimation of each atom's participation in the transition vector was obtained after performing vibrational analysis (Tables S1–S3) of the normal modes of TS0 according to the ***GF*** formalism of Wilson[75,76] and corroborated the assertion that no hydrogen migration takes place in the first step of the dissociation of AEMS.

3. Reaction routes of singlet nitrene

In addition to the nitrene intermediate, two other products were identified in the UV-PES experiments. In Sec. III B 2, we showed that the nitrene intermediate can be formed in two

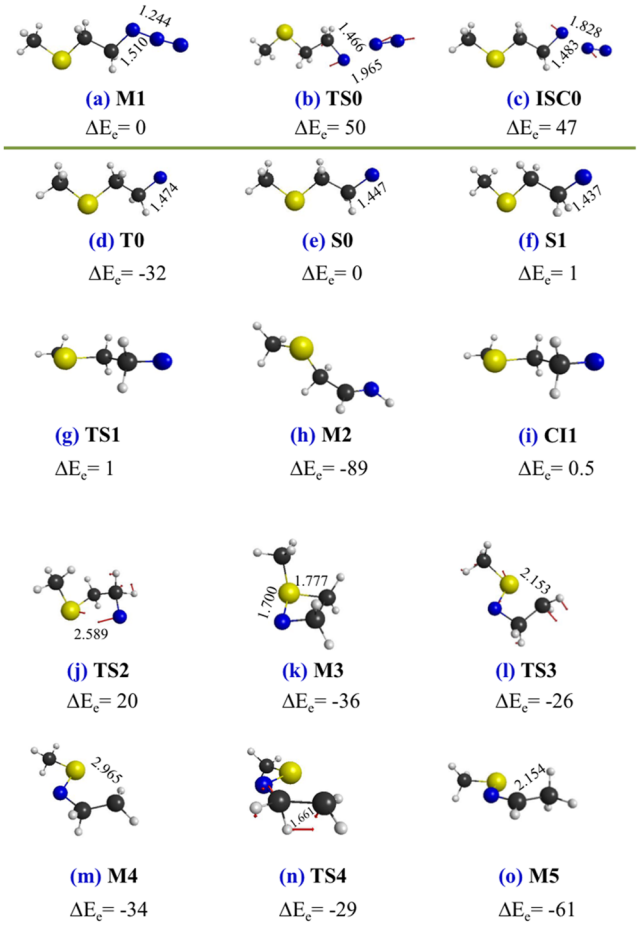

FIG. 6. CASSCF/ANO-RCC optimized geometries. (a) Azide minimum (S_0), (b) transition state for N_2 elimination (S_0), (c) intersystem crossing for N_2 elimination (S_0/T_0), (d) triplet nitrene (T_0), (e) singlet minimum (S_0), (f) singlet minimum (S_1), (g) transition state for 1,2-hydrogen shift (S_0), (h) imine, (i) conical intersection involved in 1,2-hydrogen shift, (j) transition state for cyclization of singlet minimum (S_0), (k) cycle geometry on S_0, (l) transition state for ring opening forming pseudo-carbanion (S_0), (m) pseudo-carbanion (S_0), (n) transition state for H-migration (S_0), and (o) (*Z*)-*S*-methyl-*N*-sulfenylethanimine (S_0). ΔE_e: relative electronic energy in kcal/mol.

distinct spin states, where the singlet state is the predominant product at higher temperatures. Thus, once nitrene is formed in the singlet state, two different reaction pathways are open, which lead to two different products: (a) 1,2-H shift to yield the imine derivative [2-(methylthio)ethan-1-imine (**MEI**), Fig. 6(h)] and (b) the formation of sulfenylimine [(*Z*)-*S*-methyl-*N*-sulfenylethanimine, Fig. 6(o)], which arises from a cycle intermediate that was previously formed in an almost free-barrier process starting with the singlet nitrene [Fig. 6(k)].

The molecular orbitals in the active space of the intermediates involved in such reaction channels are included in the supplementary material (Figs. S2–S6).

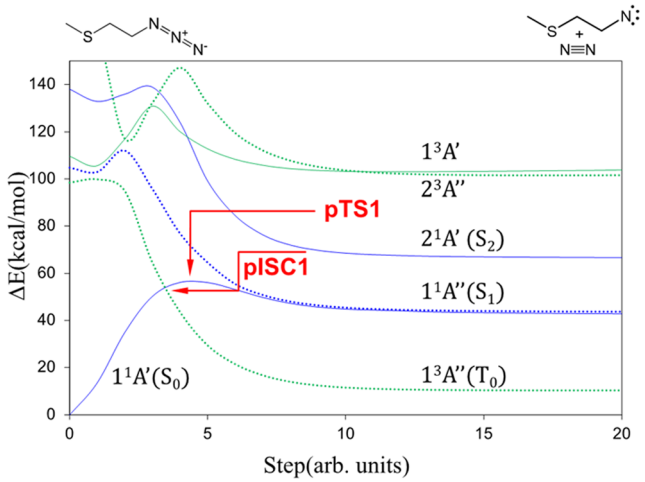

FIG. 7. MS-CASPT2 energy profiles along the interpolation line leading to dissociation of AEMS into nitrene and molecular nitrogen. Reference wavefunction *SA*2-CASSCF (16e,13o)/ANO-RCC. A′ singlet states (solid blue lines), A″ singlet state (blue dotted line), A′ triplet state (solid green line), and A″ triplet states (green dotted lines).

4. 1,2-H shift to yield the imine derivative

Starting from the singlet channel, a route with a very small barrier was found, leading to imine formation [Fig. 6(h)]. The potential energy profile of the linear interpolation connecting singlet nitrene with imine is shown in Fig. 9. This energy profile is similar to that observed for the same reaction of the nitrene derivative resulting from the decomposition of AMMS.[19] Therefore, although we could not determine the optimized geometry of the transition state involved in this reaction at the CASSCF level, we can postulate that this process is almost barrierless, analogous to the same reaction channel of AMMS, where a conical intersection [Fig. 2(i)] hinders the 1,2-hydrogen shift.

5. (Z)-S-methyl-N-sulfenylethanimine formation

The formation mechanism of sulfenylimine [**M5**, Fig. 6(o)] is depicted in Scheme 1(a) and proceeds as follows: first, a cyclic intermediate **M3** is formed from the nitrene [S_0, Fig. 6(e)] generated in the first step of the decomposition; the cyclization process has an energy barrier of ~20 kcal/mol; second, the cycle opens by breaking the S–C bond with an energy barrier of ~10 kcal/mol to generate **M4**; third, H migration gives (*Z*)-*S*-methyl-*N*-sulfenylethanimine (**M5**; energy barrier ~5 kcal/mol). **M5** can also be named *N*-ethylidene methanesulfenamide or (*Z*)-*N*-ethylidene-*S*-methylthiooxime. The transition states for these three steps were localized at the MP2/HF level, and their energies, which are included in Scheme 1(a), were reevaluated at the MS-CASPT2 level; panels (b) and (c) within the scheme represent the MS-CASPT2 energy profiles of the above reaction steps, which were obtained on top of the intrinsic reaction coordinate calculations performed at the MP2 level.

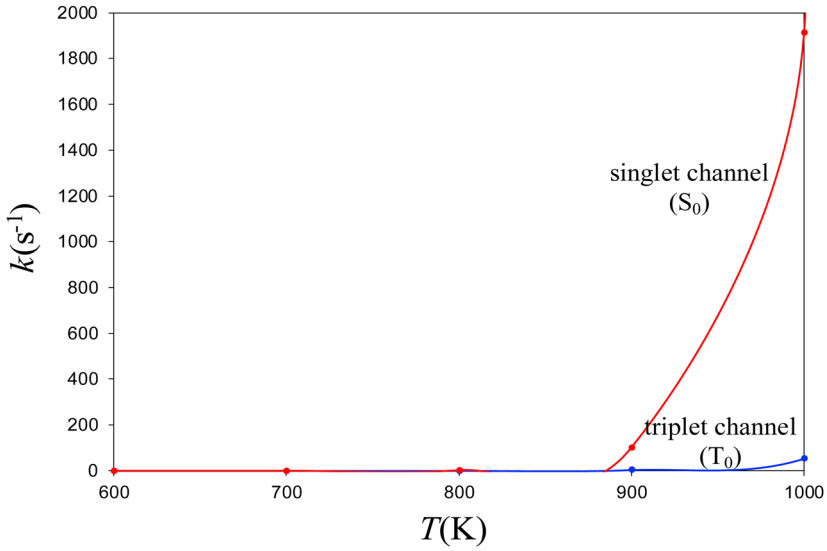

FIG. 8. Canonical rate coefficients of the singlet and triplet channels for dissociation of AEMS into nitrene and N_2 as a function of temperature.

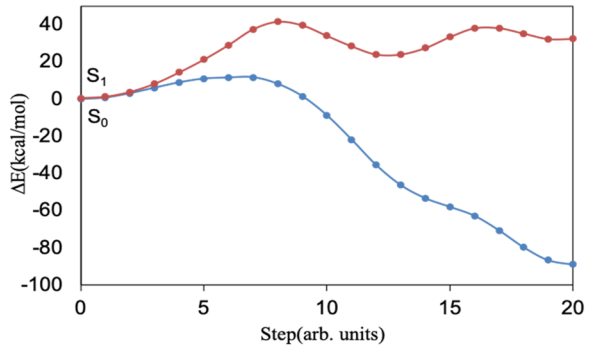

FIG. 9. MS-CASPT2 energy profiles along the interpolation line leading to isomerization of nitrene to imine. Reference wavefunction *SA*4-CASSCF(10e, 10o)/ANO-RCC.

IV. CONCLUSIONS

In summary, we studied the thermal decomposition of AEMS by means of experimental and theoretical calculations, that is, UV-PES and CASSCF and MS-CASPT2 calculations. The first step of the reaction is the dissociation of the molecule into nitrene and nitrogen. The spin state (singlet or triplet) of nitrene formed in the first step of the reaction is temperature-dependent. At low temperatures ($T \leq 650$ K), both states are formed with almost the same probability; in contrast, at high temperatures ($T \geq 1000$ K), singlet nitrene is the majority intermediate. From this singlet nitrene, three stable reaction products were detected in the experiments: an imine derivative [**M2**, Fig. 2(h)], a four-member cyclic derivative [**M3**, Fig. 2(k)], and a sulfenyl derivative [**M5**, Scheme 1(b)].

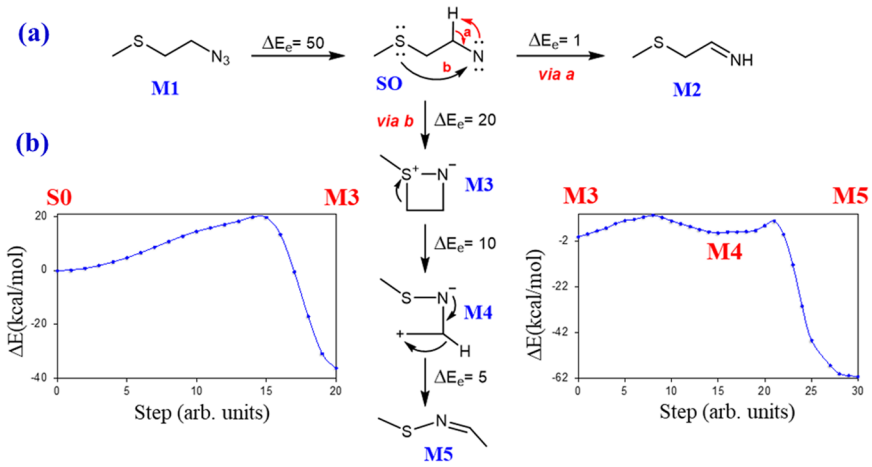

SCHEME 1. (a) Schematic representation of the decomposition channels of AEMS into (i) nitrene (**S_0**), (ii) imine (**M2**), and (iii) (*Z*)-*S*-methyl-*N*-sulfenylethanimine (**M5**). [(b) and (c)] MS-CASPT2 energy profiles for cyclization of singlet nitrene and formation of (*Z*)-*S*-methyl-*N*-sulfenylethanimine (**S_0** → **M3** → **M5**) (ΔE_e data in kcal/mol).

SUPPLEMENTARY MATERIAL

The supplementary material contains absolute energies, CASSCF molecular orbitals, and internal and Cartesian coordinates of all critical points.

ACKNOWLEDGMENTS

The authors would like to thank the Spanish Ministry of Science and Innovation (MCIN/AEI/10, Grant No. 13039/501100011033) through Project No. PID2021-122613OB-I00. J.S and M.A thank Dr. R. Larrosa and M. Guerrero for technical support in running the calculations and acknowledge the Supercomputer and Bioinformatics (SCBI) center of the University of Málaga (Spain) for computer resources. The "Direction du Numérique" of the Université de Pau et des Pays de l'Adour and Mésocentre de Calcul Intensif Aquitain (MCIA) are acknowledged for the support of computational facilities. This work received financial support from PT national funds (FCT/MCTES, Fundação para a Ciência e a Tecnologia and Ministério da Ciência, Tecnologia e Ensino Superior) through Project Nos. UIDB/50006/2020 (DOI: 10.54499/UIDB/50006/2020), UIDP/50006/2020 (DOI: 10.54499/UIDP/50006/2020), and LA/P/0140/2020 (DOI: 10.54499/LA/P/0008/2020). Authors thanks for open access charge to University of Malaga.

AUTHOR DECLARATIONS

Conflict of Interest

The authors have no conflicts to disclose.

Author Contributions

Manuel Algarra: Conceptualization (equal); Investigation (equal); Methodology (equal); Supervision (equal); Writing – original draft (equal); Writing – review & editing (equal). **Stephane Labat**: Conceptualization (equal); Investigation (equal); Methodology (equal); Supervision (equal); Writing – original draft (equal); Writing – review & editing (equal). **José Enrique Rodríguez-Borges**: Investigation (equal); Methodology (equal); Writing – original draft (equal). **María Soledad Pino-González**: Conceptualization (equal); Investigation (equal); Methodology (equal); Writing – original draft (equal); Writing – review & editing (equal). **Jean Marc Sotiropoulos**: Conceptualization (equal); Formal analysis (equal); Investigation (equal); Methodology (equal). **Juan Soto**: Conceptualization (equal); Data curation (equal); Investigation (equal); Methodology (equal); Software (equal); Validation (equal); Writing – original draft (equal).

DATA AVAILABILITY

The data that support the findings of this study are available within the article and its supplementary material.

REFERENCES

[1] M. Schock and S. Bräse, Molecules **25**, 1009 (2020).
[2] V. Paczelt, R. C. Wende, P. R. Schreiner, and A. K. Eckhardt, Angew. Chem., Int. Ed. **62**, e202218548 (2023).
[3] H. Tanimoto and K. Kakiuchi, Nat. Prod. Commun. **8**, 1021–1034 (2013).
[4] L. Bauer, M. Benz, T. M. Klapötke, T. Lenz, and J. Stierstorfer, J. Org. Chem. **86**, 6371–6380 (2021).
[5] A. Dehankar, T. Porter, J. A. Johnson, C. E. Castro, and J. O. Winter, J. Chem. Phys. **151**, 144706 (2019).
[6] J. Soto, M. Algarra, and D. Peláez, Phys. Chem. Chem. Phys. **24**, 5109–5115 (2022).
[7] A. K. Eckhardt, Chem. Commun. **58**, 8484–8487 (2022).
[8] V. D. Drabkin, V. Paczelt, and A. K. Eckhardt, Chem. Commun. **59**, 12715–12718 (2023).
[9] J. M. Dyke, G. Levita, A. Morris, J. S. Ogden, A. A. Dias, M. Algarra, J. P. Santos, M. L. Costa, P. Rodrigues, M. M. Andrade, and M. T. Barros, Chem. - Eur. J. **11**, 1665–1676 (2005).
[10] L. Craine and M. Raban, Chem. Rev. **89**, 689–712 (1989).
[11] R. Kawęcki, J. Org. Chem. **87**, 7514–7520 (2022).
[12] T. Morimoto, Y. Nezu, K. Achiwa, and M. Sekiya, J. Chem. Soc. Chem. Commun. **1985**, 1584–1585.
[13] J. Esteban, A. M. Costa, F. Urpí, and J. Vilarrasa, Tetrahedron Lett. **45**, 5563–5567 (2004).
[14] M. He, Z. Yan, F. Zhu, and S. Lin, J. Org. Chem. **83**, 15438–15448 (2018).
[15] M. Shalamu, N. Saimi, S. Luo, M. Maihemuti, and A. Abudu Rexit, J. Org. Chem. **89**, 3696–3701 (2024).
[16] Q. Wang, H. Mei, R. Pajkert, G. V. Röschenthaler, and J. Han, Tetrahedron **162**, 134133 (2024).
[17] S. Roy, K. A. Unnikrishnan, A. Chakraborty, R. Kuniyil, and I. Chatterjee, Org. Lett. **26**, 1629–1634 (2024).
[18] M. Algarra, J. Soto, L. Pinto da Silva, M. S. Pino-González, J. E. Rodríguez-Borges, J. Mascetti, F. Borget, A. Reisi-Vanani, and R. Luque, J. Phys. Chem. A **124**, 1911–1921 (2020).
[19] M. J. Frisch, G. W. Trucks, H. B. Schlegel, G. E. Scuseria, M. A. Robb, J. R. Cheeseman, G. Scalmani, V. Barone, G. A Petersson, H. Nakatsuji, X. Li, M. Caricato, A. V. Marenich, J. Bloino, B. G. Janesko, R. Gomperts, B. Mennucci, H. P. Hratchian, J. V. Ortiz, A. F. Izmaylov, J. L. Sonnenberg, D. Williams-Young, F. Ding, F. Lipparini, F. Egidi, J. Goings, B. Peng, A. Petrone, T. Henderson, D. Ranasinghe, V. G. Zakrzewski, J. Gao, N. Rega, G. Zheng, W. Liang, M. Hada, M. Ehara, K. Toyota, R. Fukuda, J. Hasegawa, M. Ishida, T. Nakajima, Y. Honda, O. Kitao, H. Nakai, T. Vreven, K. Throssell, J. A. Montgomery, Jr., J. E. Peralta, F. Ogliaro, M. J. Bearpark, J. J. Heyd, E. N. Brothers, K. N. Kudin, V. N. Staroverov, T. A. Keith, R. Kobayashi, J. Normand, K. Raghavachari, A. P. Rendell, J. C. Burant, S. S. Iyengar, J. Tomasi, M. Cossi, J. M. Millam, M. Klene, C. Adamo, R. Cammi, J. W. Ochterski, R. L. Martin, K. Morokuma, O. Farkas, J. B. Foresman, and D. J. Fox, *Gaussian 16, Revision C.01*, Gaussian, Inc., Wallingford, CT, 2016.
[20] A. D. Becke, Phys. Rev. A **38**, 3098–3100 (1988).
[21] A. D. Becke, J. Chem. Phys. **98**, 5648 (1993).
[22] C. Lee, W. Yang, and R. G. Parr, Phys. Rev. B **37**, 785–789 (1988).
[23] T. Yanai, D. P. Tew, and N. C. A. Hand, Chem. Phys. Lett. **393**, 51–57 (2004).
[24] R. Krishnan, J. S. Binkley, R. Seeger, and J. A. Pople, J. Chem. Phys. **72**, 650–654 (1980).
[25] H. M. Muchall, N. H. Werstiuk, B. Choudhurry, J. Ma, J. Warkentin, and J. P. Pezacki, Can. J. Chem. **76**, 238–240 (1998).
[26] H. M. Muchall and P. Rademacher, J. Mol. Struct. **471**, 189–194 (1998).
[27] B. O. Roos, P. R. Taylor, and P. E. M. Siegbahn, Chem. Phys. **48**, 157–173 (1980).
[28] B. O. Roos, Int. J. Quantum Chem. **18**, 175–189 (2009).
[29] H. J. Werner and W. Meyer, J. Chem. Phys. **73**, 2342–2356 (1980).
[30] P. E. M. Siegbahn, J. Almlöf, A. Heiberg, and B. O. Roos, J. Chem. Phys. **74**, 2384–2396 (1981).
[31] H. J. Werner and W. Meyer, J. Chem. Phys. **74**, 5794 (1981).
[32] B. O. Roos, in *Advances in Chemical Physics, Ab Initio Methods in Quantum Chemistry II*, edited by K. P. Lawley (John Wiley & Sons, Chichester, UK, 1987), Chap. 69, p. 399.
[33] J. Olsen, Int. J. Quantum Chem. **111**, 3267–3272 (2011).
[34] B. O. Roos, K. Andersson, M. P. Fülscher, P. A. Malmqvist, L. Serrano-Andrés, K. Pierloot, and M. Merchán, Adv. Chem. Phys. **93**, 219 (1996).
[35] J. Finley, P.-Å. Malmqvist, B. O. Roos, and L. Serrano-Andrés, Chem. Phys. Lett. **288**, 299–306 (1998).
[36] V. Veryazov, P. O. Widmark, L. Serrano-Andrés, R. Lindh, and B. O. Roos, Int. J. Quantum Chem. **100**, 626–635 (2004).

[37]F. Aquilante, J. Autschbach, R. K. Carlson, L. F. Chibotaru, M. G. Delcey, L. De Vico, I. Fdez Galván, N. Ferré, L. M. Frutos, L. Gagliardi, M. Garavelli, A. Giussani, C. E. Hoyer, G. Li Manni, H. Lischka, D. Ma, P.-Å. Malmqvist, T. Müller, A. Nenov, M. Olivucci, T. B. Pedersen, D. Peng, F. Plasser, B. Pritchard, M. Reiher, I. Rivalta, I. Schapiro, J. Segarra-Martí, M. Stenrup, D. G. Truhlar, L. Ungur, A. Valentini, S. Vancoillie, V. Veryazov, V. P. Vysotskiy, O. Weingart, F. Zapata, and R. Lindh, "Molcas 8: New capabilities for multiconfigurational quantum chemical calculations across the periodic table," J. Comput. Chem. **37**, 506–541 (2016); I. Fdez Galván, M. Vacher, A. Alavi, C. Angeli, F. Aquilante, J. Autschbach, J. J. Bao, S. I. Bokarev, N. A. Bogdanov, R. K. Carlson, L. F. Chibotaru, J. Creutzberg, N. Dattani, M. G. Delcey, S. S. Dong, A. Dreuw, L. Freitag, L. M. Frutos, L. Gagliardi, F. Gendron, A. Giussani, L. González, G. Grell, M. Guo, C. E. Hoyer, M. Johansson, S. Keller, S. Knecht, G. Kovacević, E. Källman, G. Li Manni, M. Lundberg, Y. Ma, S. Mai, J. P. Malhado, P. Å. Malmqvist, P. Marquetand, S. A. Mewes, J. Norell, M. Olivucci, M. Oppel, Q. M. Phung, K. Pierloot, F. Plasser, M. Reiher, A. M. Sand, I. Schapiro, P. Sharma, C. J. Stein, L. K. Sørensen, D. G. Truhlar, M. Ugandi, L. Ungur, A. Valentini, S. Vancoillie, V. Veryazov, O. Weser, T. A. Wesołowski, P.-O. Widmark, S. Wouters, A. Zech, J. P. Zobel, and R. Lindh, J. Chem. Theory Comput. **15**, 5925–5964 (2019).
[38]I. Fdez Galván, M. G. Delcey, T. B. Pedersen, F. Aquilante, and R. Lindh, J. Chem. Theory Comput. **12**, 3636–3653 (2016).
[39]B. O. Roos, R. Lindh, P.-Å. Malmqvist, V. Veryazov, and P. O. Widmark, J. Phys. Chem. A **108**, 2851–2858 (2004).
[40]B. O. Roos, R. Lindh, P.-Å. Malmqvist, V. Veryazov, and P. O. Widmark, J. Phys. Chem. A **109**, 6575–6579 (2005).
[41]A. R. Allouche, J. Comput. Chem. **32**, 174–182 (2011).
[42]G. Schaftenaar and J. H. Noordik, J. Comput.-Aided Mol. Des. **14**, 123–134 (2000).
[43]B. M. Bode and M. S. Gordon, J. Mol. Graphics Modell. **16**, 133–138 (1998).
[44]B. A. Heß, C. M. Marian, U. Wahlgren, and O. Gropen, Chem. Phys. Lett. **251**, 365–371 (1996).
[45]P. A. Malmqvist, B. O. Roos, and B. Schimmelpfenning, Chem. Phys. Lett. **357**, 230–240 (2002).
[46]C. Ribbing, B. Gilliams, K. Pierloot, B. O. Roos, and G. Karlström, J. Chem. Phys. **109**, 3145–3152 (1998).
[47]D. Peláez, J. F. Arenas, J. C. Otero, and J. Soto, J. Chem. Phys. **125**, 164311 (2006).
[48]J. Soto, J. Phys. Chem. A **127**, 9781–9786 (2023).
[49]J. Soto, J. Phys. Chem. A **126**, 8372–8379 (2022).
[50]J. Soto, D. Peláez, and M. Algarra, J. Chem. Phys. **158**, 204301 (2023).
[51]D. R. Glowacki, C. H. Liang, C. Morley, M. J. Pilling, and S. H. Robertson, J. Phys. Chem. A **116**, 9545–9560 (2012).
[52]P. Pokhilko, R. Shannon, D. Glowacki, H. Wang, and A. I. Krylov, J. Phys. Chem. A **123**, 482–491 (2019).
[53]L. Onel, R. Lade, J. Mortiboy, M. A. Blitz, P. W. Seakins, D. E. Heard, and D. Stone, Phys. Chem. Chem. Phys. **23**, 19415–19423 (2021).
[54]Z. S. Mir, T. R. Lewis, L. Onel, M. A. Blitz, P. W. Seakins, and D. Stone, Phys. Chem. Chem. Phys. **22**, 9448–9459 (2020).
[55]D. J. Medeiros, S. H. Robertson, M. A. Blitz, and P. W. Seakins, J. Phys. Chem. A **124**, 4015–4024 (2020).
[56]C. Zener, Proc. R. Soc. London, Ser. A **137**, 696–702 (1932).
[57]L. D. Landau, Phys. Z. Sowjetunion **2**, 46–51 (1932).
[58]O. K. Rice and H. C. Ramsperger, J. Am. Chem. Soc. **49**, 1617–1629 (1927).
[59]L. S. Kassel, J. Phys. Chem. **32**, 225–242 (1928).
[60]L. S. Kassel, J. Phys. Chem. **32**, 1065–1079 (1928).
[61]R. A. Marcus and O. K. Rice, J. Phys. Chem. **55**, 894–908 (1951).
[62]R. A. Marcus, J. Chem. Phys. **43**, 2658–2661 (1965).
[63]D. Aranda, F. J. Avila, I. López-Tocón, J. F. Arenas, J. C. Otero, and J. Soto, Phys. Chem. Chem. Phys. **20**, 7764–7771 (2018).
[64]J. Soto, J. C. Otero, F. J. Avila, and D. Peláez, Phys. Chem. Chem. Phys. **21**, 2389–2396 (2019).
[65]M. Algarra and J. Soto, ChemPhysChem **21**, 1126–1133 (2020).
[66]D. Mu and Q. S. Li, Phys. Chem. Chem. Phys. **25**, 8074–8081 (2023).
[67]X. L. Peng, A. Migani, Q. S. Li, Z. S. Li, and L. Blancafort, Phys. Chem. Chem. Phys. **20**, 1181–1188 (2018).
[68]D. A. Kreplin, P. J. Knowles, and H. J. Werner, J. Chem. Phys. **150**, 194106 (2019).
[69]D. A. Kreplin, P. J. Knowles, and H. J. Werner, J. Chem. Phys. **152**, 074102 (2020).
[70]J. Soto and J. C. Otero, J. Phys. Chem. A **123**, 9053–9060 (2019).
[71]J. Soto, D. Peláez, and J. C. Otero, J. Chem. Phys. **154**, 044307 (2021).
[72]M. Bixon and J. Jortner, J. Chem. Phys. **48**, 715 (1968).
[73]S. D. Colson and E. R. Bernstein, J. Chem. Phys. **43**, 2661–2669 (1965).
[74]V. Weisskopfand and E. Wigner, Z. Phys. **63**, 54–73 (1930).
[75]E. B. Wilson, Jr., J. C. Decius, and P. C. Cross, *Molecular Vibrations* (McGraw-Hills, New York, 1955).
[76]J. F. Arenas, S. P. Centeno, J. I. Marcos, J. C. Otero, and J. Soto, J. Chem. Phys. **113**, 8472–8477 (2000).